**International Journal of Power Electronics and Drive System (IJPEDS)**
Vol. 17, No. 4, December 2026, pp. 2806~2815
ISSN: 2088-8694, DOI: 10.11591/ijpeds.v17.i4.pp2806-2815 

# An adaptive fuzzy-SMC based active voltage balancing circuit for high rating EV battery pack

**Pravin Sakharam Wankhade, Prema Manoj Daigavane**
Department of Electrical Engineering, Raisoni Centre for Research and Innovation, G. H. Raisoni University, Amravati, India

**Article Info**

***Article history:***

Received Apr 19, 2026
Revised Sep 10, 2026
Accepted Sep 17, 2026

***Keywords:***

Adaptive neuro fuzzy inference system
Electric vehicle
Proportional integral
Sliding mode control
State of charge

**ABSTRACT**

In order to increase the lifespan and charge/discharge cycles of the battery, the state of charge (SOC) of each cell in the battery pack of the electric vehicle (EV) has to be maintained the same. Especially in high-rating battery pack EVs with larger storage capacity and higher voltage, cell voltage balancing is mandatory. With equal voltages of the cells, charging or discharging also happens in a balanced structure, maintaining the SOC of all cells at the same value. In order to achieve this, passive or active voltage balancing circuits are needed. In this paper, an active balancing circuit is proposed with a full bridge controlled by an adaptive fuzzy-SMC voltage regulator. In this regulator, the gains of the sliding mode control (SMC) are varied by fuzzy logic control with two input variables. Here, the sliding variable in the controller is the error signal generated by the comparison of the reference and measured signals. The gains of the SMC Ki and Kq are varied by the fuzzy control with 25 rules base for each gain. The SMC is tuned as per the response of the voltage balancing circuit, keeping the ripple of the battery current very low. A comparative analysis is done with different regulators, including conventional proportional-integral (PI) and adaptive neuro fuzzy inference system (ANFIS) regulators. The peak overshoot, settling time, and the ripple in the battery current are compared to validate the optimal regulator for the active voltage balancing circuit.

*This is an open access article under the CC BY-SA license.*

***Corresponding Author:***

Pravin Sakharam Wankhade
Department of Electrical Engineering, Raisoni Centre for Research and Innovation
G. H. Raisoni University
Amravati, Maharashtra, India
Email: pravinwankhade512@gmail.com

## 1. INTRODUCTION

Global temperatures are rising across many locations due to pollution from electrical power generation and transportation. The pollution caused by electrical power generation is mitigated using renewable and hybrid sources. The major remaining contribution comes from transportation vehicles. The conventional internal combustion engine (ICE) vehicles burn petroleum fuel and exhaust hazardous gases affecting the environment. These ICE vehicles need to be replaced by pure electric vehicles (EVs) with zero tailpipe emissions, supporting carbon-neutral and sustainable economies [1].

During charging, renewable sources store power in the cells of the pure EV battery pack through power electronic circuits, and this stored energy drives the vehicle [2], [3]. Stable charging requires attention to several factors, and in modern EV technology, the battery management system (BMS) plays a crucial role in maintaining vehicle life and reliability [4]. State of charge (SOC), individual cell voltage, and module temperature must all be considered and continuously monitored in real time for balanced and optimal charging [5]. Advanced intelligent BMS technology has adaptive and hybrid controllers for maintaining the battery pack temperature at limited levels during charging/discharging. However, cell voltage balancing

cannot be achieved by control modules an active voltage balancing circuit is connected to the battery pack [4]. The switches in this active voltage balancing circuit are controlled by the BMS module with adaptive controllers for optimal stability of the cells. Some of the active balancing circuits are presented in Figure 1, which control the cell voltage [5].

Advanced intelligent BMS technology uses adaptive and hybrid controllers to keep the battery pack temperature within limits during charging/discharging. However, cell voltage balancing cannot be achieved by control modules alone, so an active voltage balancing circuit is connected to the battery pack [6], with its switches driven by the BMS through adaptive controllers. Typical active balancing circuits are presented in Figure 1 [7]. In the inductor-based circuit of Figure 1(a), MOSFET switches control the charge and discharge of multiple inductors placed equally between the cells [8]. The transformer-based circuit of Figure 1(b) [9] adds mutual inductance storage, and its turns ratio can be changed as required to enhance voltage balancing of the cells. In the capacitor-based circuit of Figure 1(c), capacitors are connected in a mesh with MOSFET switches between the battery cells [10]; switching changes the charging of the capacitors and balances the cell voltages. These conventional circuits have been further developed with hybrid passive elements, as presented in Figure 2.

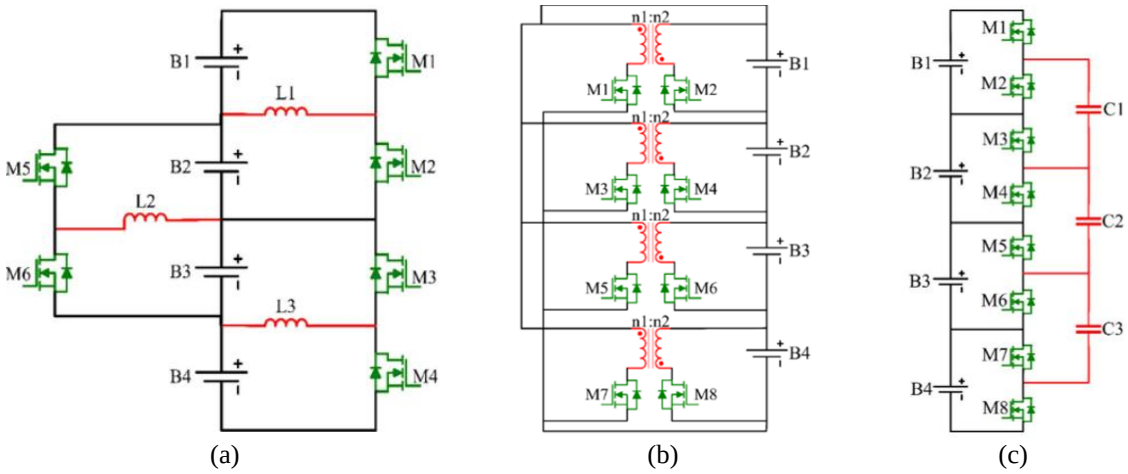


(a) (b) (c)

Figure 1. Active voltage balancing circuits: (a) inductor-based, (b) transformer-based, and (c) capacitor-based

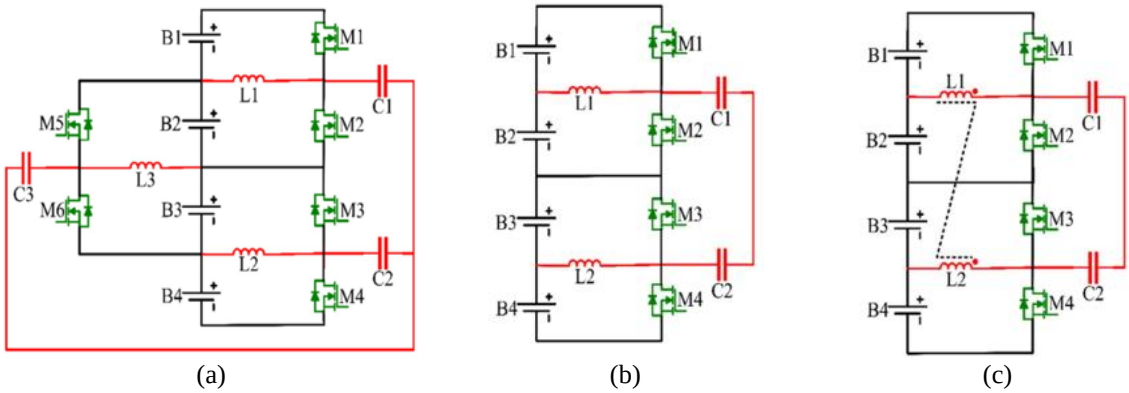


(a) (b) (c)

Figure 2. Hybrid active balancing circuit: (a) interleaved buck–boost, (b) series buck–boost, and (c) coupled inductors buck–boost

Figure 2 shows inductor–capacitor topologies for better cell balance [11]: the interleaved buck–boost circuit of Figure 2(a) shares the balancing current between two inductor paths, the series buck–boost circuit of Figure 2(b) moves charge between adjacent cells through series LC branches, and the coupled-inductor circuit of Figure 2(c) integrates mutual inductance and suits higher power ratings. Transformer-based circuits are safer since the transformer isolates the cells from the input source [12]. This paper therefore proposes a full-bridge, high-frequency transformer-based voltage balancing circuit. Because the conventional PI regulator has very low damping and creates oscillations and overshoots, it is replaced by a

fuzzy–SMC regulator that reduces ripple and initial overshoot, while the 'constant current' charging scheme controls the switch duty ratio. Such AI-driven adaptive strategies are increasingly adopted to optimize performance in modern energy and communication infrastructures [13]. Table 1 compares the regulators used in EV battery charging control. The rest of this paper is organized as follows: i) Section 2 presents the proposed FBPS topology and its control module; ii) Section 3 details the adaptive fuzzy sliding mode controller design; iii) Section 4 presents simulation results comparing regulators; and iv) Section 5 concludes with validation of ripple and voltage balancing performance.

Table 1. Regulators comparison

| Feature | PI | ANFIS | SMC | Fuzzy – SMC |
|---|---|---|---|---|
| Dynamic response | Moderate | Fast | Very fast | Ultra-fast |
| Overshoot | Medium | Low | Low | Very low |
| Type | Linear controller | Adaptive intelligent | Non-linear controller | Hybrid intelligent and non-linear |
| Robustness | Low | Moderate | High | Very high |
| Mathematical model | Needed | Not required (tool-based design) | Needed | Partly needed |
| Tuning | Easy | Difficult | Medium | Difficult |
| Stability | Moderately stable | Good | Good | Excellent |
| Applications | Linear systems | Non-linear systems | Non-linear systems | Linear or extreme uncertain non-linear system |

## 2. PROPOSED VOLTAGE BALANCING CIRCUIT

The proposed voltage balancing circuit is a 'full bridge phase shift' (FBPS) converter [14], [15] designed using two full bridges [11]. One bridge includes all MOSFET switches that can be controlled, and the other bridge is an uncontrolled diode bridge. The MOSFET-based full bridge is connected on the primary side, and the uncontrolled diode bridge is connected on the secondary side of the high-frequency transformer [12]. The complete circuit structure of the proposed FBPS is presented in Figure 3.

As presented in Figure 3, the proposed converter combines a transformer, inductance, capacitance, and active switches, making it more efficient and stable than conventional circuits. The input DC source is obtained from an AC/DC charger connected to a 1-ph or 3-ph AC supply [16]. The MOSFET bridge converts this DC supply to a high-frequency AC voltage, which is induced to the secondary side through the n1:n2 turns ratio transformer, rectified by the uncontrolled diode bridge (D9-D12) and fed to the first cell B1 through inductor L2 [17]. The secondary voltage magnitude is controlled by the duty ratio of the MOSFET switches.

The duty ratio of the MOSFET switches included in FBPS is controlled by constant voltage-based control. The controller takes feedback from the cell voltages of all the cells and considers the average of the voltages ($V_{cell\ avg}$).

$$V_{cell\ avg} = V_{cell1} + V_{cell2} + \cdots + V_{celln} \tag{1}$$

The average measured cell voltage is compared to a reference value, which is the maximum cell voltage, and the resulting error is fed to the regulator to generate the duty ratio of the MOSFET switches [18]. The control structure of the proposed system is presented in Figure 4. As per the given Figure 4, the duty ratio (D) generated by the regulator is compared to a sawtooth waveform, which generates PWM pulses from the PWM generator. The duty ratio generated by the PI regulator is given as (2).

$$D = \left(V_{ref} - V_{cell\ avg}\right)\left(K_p + \frac{K_i}{s}\right) \tag{2}$$

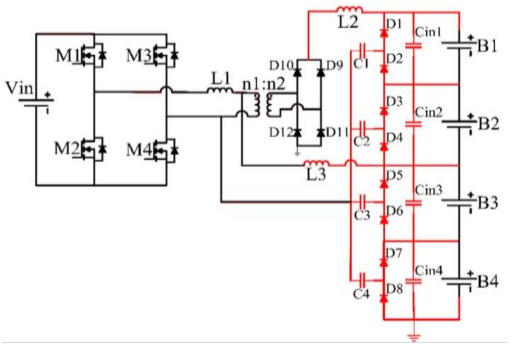


Figure 3. FBPS voltage balancing circuit

The PWM pulse is fed directly to switches M1 and M4, and its complement (NOT gate) to M2 and M3 of the FBPS converter [19]. The conventional proportional integral (PI) regulator has very low damping and creates high ripple in the cell charging currents [20], which degrades the cells and reduces the life of the battery pack. It therefore needs to be replaced by an adaptive regulator whose gains change with the error signal, as designed in the following section.

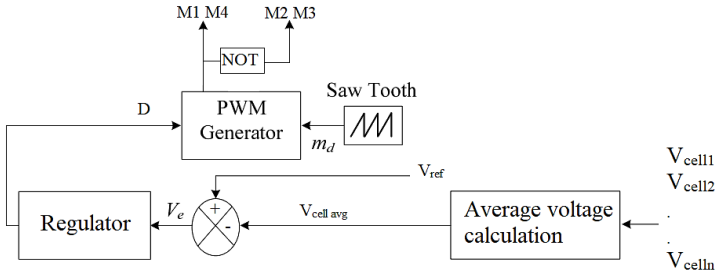


Figure 4. Control structure of the proposed FBPS converter

## 3. ADAPTIVE FUZZY SLIDING MODE CONTROL DESIGN

The adaptive fuzzy sliding mode control is an advancement over the conventional PI and ANFIS regulators, which are modelled with low damping and therefore create more ripple and disturbances in the system [21], reducing the reliability of the cells and the life of the battery pack. The proposed regulator adapts to changes in the cell characteristics, even under sudden variations in the charging conditions [22]. Its internal structure is presented in Figure 5.

As presented in Figure 5 the second order sliding mode controller is integrated with Fuzzy module which generates the gains 'Ki' and 'Kq' of the sliding mode controller [20]. The values of 'Ki' and 'Kq' gains depends on the sliding variable 'Sw' which is generated by the comparison of reference voltage ($V_{ref}$) and measured average cell voltage ($V_{avg}$). The sliding variable and duty ratio are expressed as (3) and (4).

$$S_\omega = V_{ref} - V_{cell\ avg} \tag{3}$$

$$D = \left(\widetilde{K_q}.\sqrt{|S_\omega|}\right) + \left(\frac{\widetilde{K_l}.tanhtanh\,(S_\omega)}{s}\right) \tag{4}$$

Here, $\widetilde{K_l}$ and $\widetilde{K_q}$ are the variable integral gain and quality factor gain which are generated by the Fuzzy logic tool with specific membership functions (MFs) and rule base for the MFs [21]. The input to the Fuzzy module is the sliding variable (Sw) by which change in sliding variable is also determined by 'unit delay'. The comparison of present and previous value of the $S_\omega$ variable generates the change in sliding variable ($dS_\omega$).

$$dS_\omega = S_\omega(t) - S_\omega(t-1) \tag{5}$$

Each input variable is set with five MFs and the output variable is set with three MFs which are linked with IF-THEN rule base [22]. The MFs of the input ($S_\omega$and $dS_\omega$) and output (D) variables are presented in Figure 6.

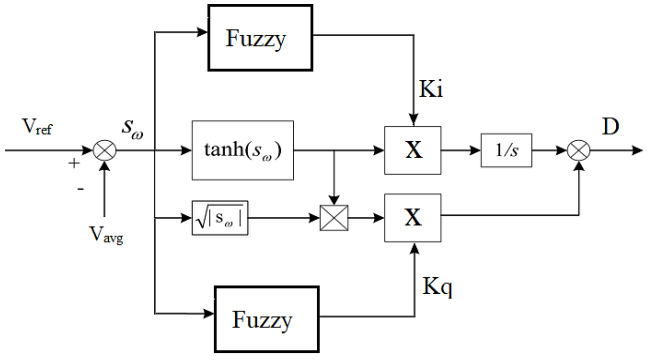


Figure 5. Adaptive fuzzy sliding mode control structure

As presented in Figure 6, triangular MFs are used to maintain precision in the gain values [23]-[25]. The $S_\omega$ variable ranges from -10 to 10 and the $dS_\omega$ variable from -1 to 1; these are the maximum input limits allowed by the fuzzy design to decrease the response time [26], since a lower range limits the output during transient states. The Ki output ranges from 0 to 0.01 and Kq from 0 to 0.5. The MFs are named by their position in the range [27]: big negative (BN), medium negative (MN), zero (Z), medium positive (MP), and big positive (BP). To reduce complexity, the output variable has only three MFs: small (S), medium (M), and big (B) [28]. The input and output variables are linked by the IF-THEN rule bases in Tables 2 and 3, which generate the gain values according to the region of the input variables.

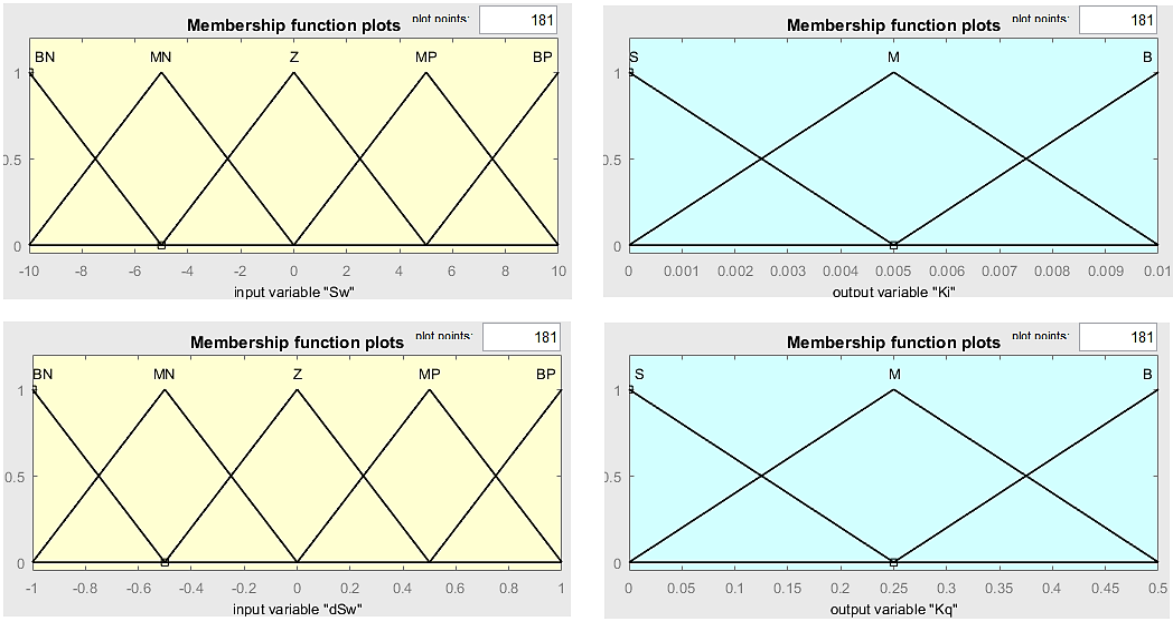


Figure 6. MFs of input and output variables

Table 2. '$\widetilde{K_i}$' gain rule base

| $\widetilde{K_i}$ | | Variable 'Sw' | | | | |
|---|---|---|---|---|---|---|
| | | BP | MP | Z | MN | BN |
| Variable 'dSw' | BP | B | B | S | B | B |
| | MP | B | B | S | B | B |
| | Z | B | M | M | M | B |
| | MN | B | B | S | B | B |
| | BN | B | B | S | S | B |

Table 3. '$\widetilde{K_q}$' gain rule base

| $\widetilde{K_q}$ | | Variable 'Sw' | | | | |
|---|---|---|---|---|---|---|
| | | BP | MP | Z | MN | BN |
| Variable 'dSw' | BP | B | M | S | M | B |
| | MP | B | M | M | M | B |
| | Z | B | B | M | B | B |
| | MN | B | M | M | M | B |
| | BN | B | M | S | M | B |

## 4. SIMULATION RESULT ANALYSIS

The proposed FBPS voltage balancing circuit is modelled in MATLAB Simulink using the 'Powersystems' tools. Four battery cells with different SOC levels are considered, so that different charging currents are required for voltage balancing. The primary-side full bridge is controlled by the constant voltage controller using the average cell voltage. Results recorded with the PI regulator are compared with those of the ANFIS and adaptive fuzzy SMC regulators. The circuit parameters are presented in Table 4.

Table 4. Topology parameters

| Name of the module | Parameters |
|---|---|
| Vin | 600 Vdc |
| Voltage balancing circuit | $R_{mosfet}$ = 1 mΩ, L1 = 3 µH, C = 1 mF, $n_{HFT}$ = 2 fc = 50 kHz |
| Battery | Vbat = 72 V, Capacity = 40 Ah |
| | $SOC_{int}1$ = 40%; $SOC_{int}2$ = 60%; $SOC_{int}3$ = 20%; $SOC_{int}4$ = 80%; |
| PI regulator | Kp = 0.05, Ki = 0.00023, fc= 50 kHz |
| Adaptive fuzzy SMC | $\widetilde{K_i}$ range : 0 to 0.01 |
| | $\widetilde{K_q}$ range : 0 to 0.5 |
| | $S_\omega$ range : -10 to 10 |
| | $dS_\omega$ range : -1 to 1 |

The AF-SMC regulator is built with blocks from the 'Continuous', 'Discrete', 'Math functions' and fuzzy toolbox of the Simulink library, as presented in Figure 7. The 3-dimensional plots of the input and output variables for the given MFs and rule base are presented in Figure 8, and the resulting Ki and Kq gains, which depend on the region of the input variables generated by comparing the reference and measured voltages, are presented in Figure 9.

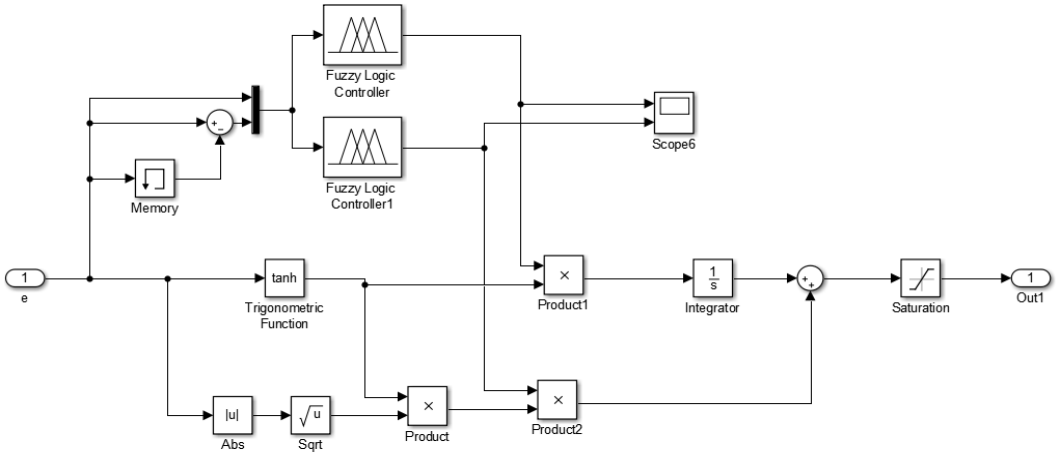


Figure 7. Adaptive fuzzy based SMC regulator modeling

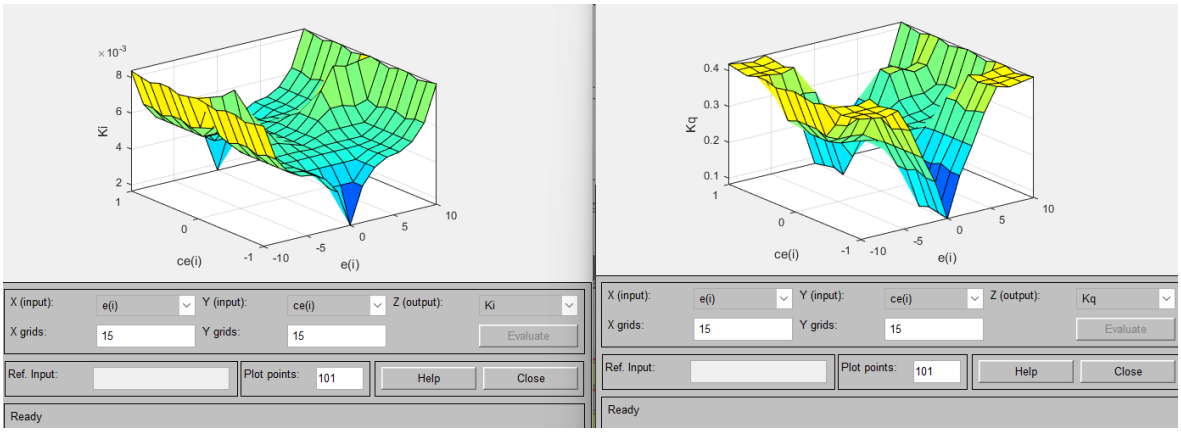


Figure 8. 3-dimensional plotting of the fuzzy gains

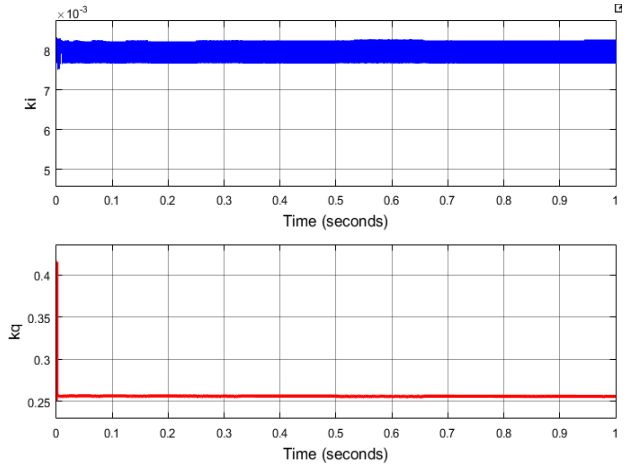


Figure 9. Ki and Kq gains from fuzzy modules

As illustrated in Figure 10, the transformer voltage drops from 300 V on the primary to 150 V on the secondary owing to the reduced secondary turns; this voltage is rectified by the diode bridge to charge the battery cells. To create uneven cell voltages, different initial SOCs are set, and Figure 11 shows these SOCs rising as the cells charge. Owing to the different initial SOCs, the initial cell voltages in Figure 12 also differ and are equalized at 0.8ms by the voltage balancing topology, which is achieved through different charging current magnitudes. As observed in Figure 13, the charging currents differ according to the initial SOC, and the ripple in the current is drastically reduced when the regulator is replaced with AF-SMC. The parametric comparison of the regulators in Table 5 validates the proposed regulator for the topology.

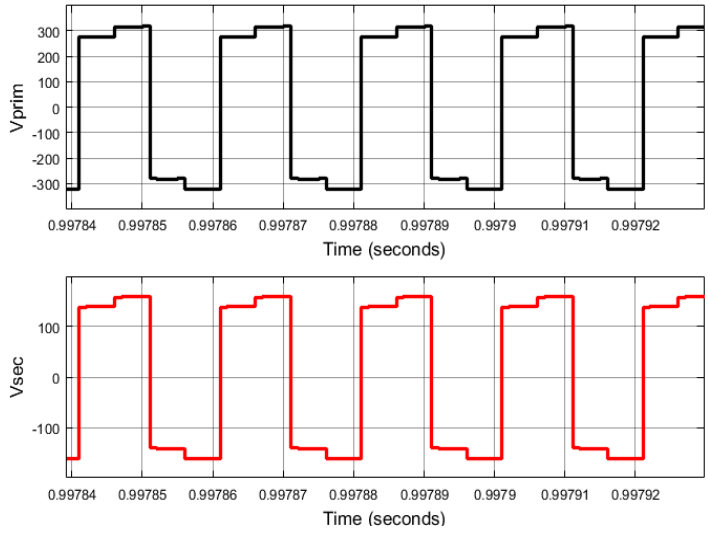


Figure 10. Primary/secondary transformer voltage

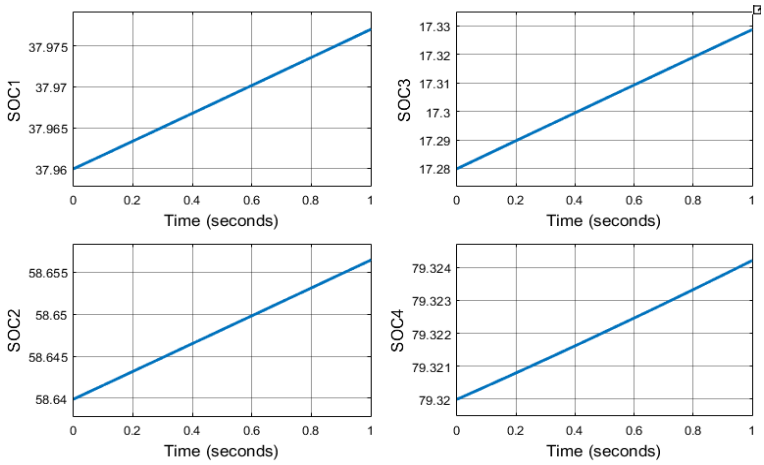


Figure 11. SOCs of the battery cells

Table 5. Comparison table

| Parameter | PI | ANFIS | AF-SMC |
|---|---|---|---|
| Initial peak overshoot – Ibat 1 | 47 A | 30 A | 26 A |
| Ripple – Ibat 1 | 27.8% | 3% | 1.8% |
| Initial peak overshoot – Ibat 2 | 40 A | 38 A | 29 A |
| Ripple – Ibat 2 | 79% | 11.5% | 7.2% |
| Initial peak overshoot – Ibat 3 | 100 A | 88 A | 74 A |
| Ripple – Ibat 3 | 33.8% | 8.5% | 5.6% |
| Initial peak overshoot – Ibat 4 | 10 A | 3 A | 2 A |
| Ripple – Ibat 4 | 90% | 8% | 4.8% |

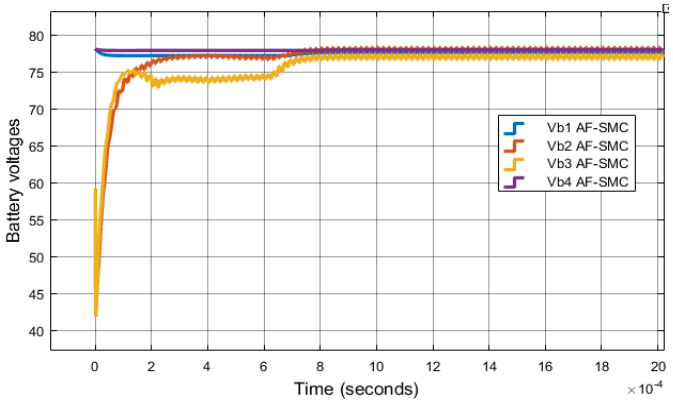


Figure 12. Voltages of the battery cells

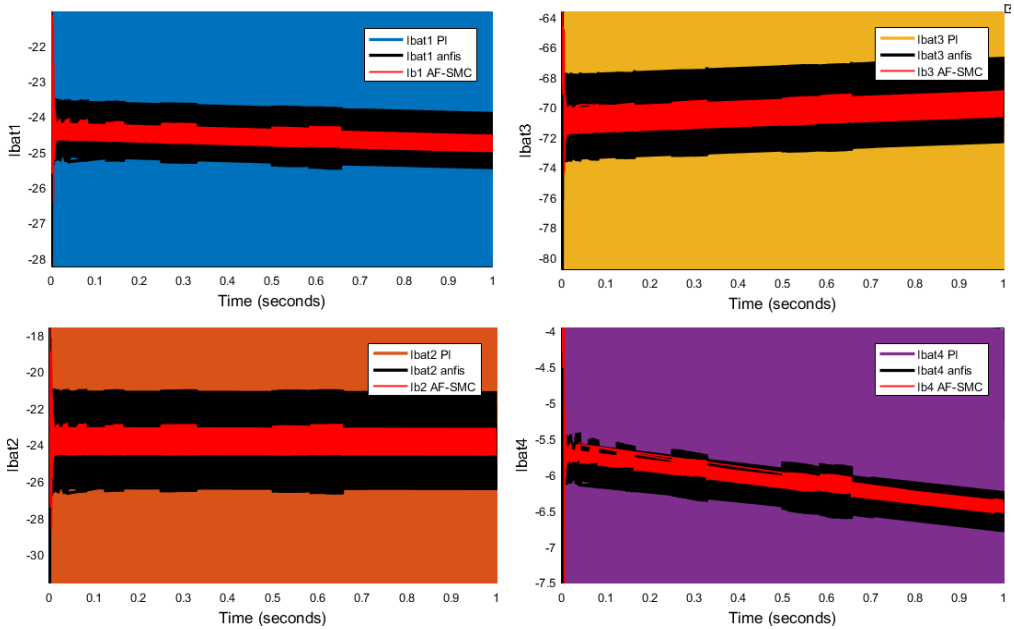


Figure 13. Charging currents of the battery cells

## 5. CONCLUSION

Among voltage balancing circuits based on passive elements, active elements, transformers, and hybrid circuits, the proposed FBPS is more efficient and stable, as validated by MATLAB Simulink modelling. Despite different initial SOCs, the cells are balanced by charging them with different current magnitudes, with the MOSFET duty ratio generated from the average cell voltage error. The AF-SMC regulator gives about 50% lower ripple and 20% lower initial peak overshoot than the PI and ANFIS regulators. Since further optimization-based regulators are too complex and costly for practical chargers, the proposed topology uses adaptive and hybrid regulators that keep charger cost low.

## ACKNOWLEDGMENTS

The authors gratefully acknowledge Jagadambha College of Engineering & Technology, Yavatmal, and G.H. Raisoni University, Amravati, for the facilities and support extended during this work. This research did not receive any specific research grant or contract from funding agencies in the public, commercial, or not-for-profit sectors.

## FUNDING INFORMATION

The authors state no funding involved.

## AUTHOR CONTRIBUTIONS STATEMENT

This journal uses the Contributor Roles Taxonomy (CRediT) to recognize individual author contributions, reduce authorship disputes, and facilitate collaboration.

| Name of Author | C | M | So | Va | Fo | I | R | D | O | E | Vi | Su | P | Fu |
|---|---|---|---|---|---|---|---|---|---|---|---|---|---|---|
| Pravin Sakharam Wankhade | ✓ | ✓ | ✓ | ✓ | ✓ | ✓ | | | ✓ | | ✓ | | | |
| Prema Manoj Daigavane | ✓ | ✓ | | | | | ✓ | | | ✓ | | ✓ | ✓ | |

C : **C**onceptualization
M : **M**ethodology
So : **So**ftware
Va : **Va**lidation
Fo : **Fo**rmal analysis
I : **I**nvestigation
R : **R**esources
D : **D**ata Curation
O : Writing - **O**riginal Draft
E : Writing - Review & **E**diting
Vi : **Vi**sualization
Su : **Su**pervision
P : **P**roject administration
Fu : **Fu**nding acquisition

## CONFLICT OF INTEREST STATEMENT

The authors declare that they have no conflict of interest.

## DATA AVAILABILITY

The data supporting the findings of this study (MATLAB Simulink model and simulation results) are available from the corresponding author upon reasonable request.

## REFERENCES


[1] B. V. Kumar, J. Sharma, K. R. Anne, S. Khan, M. Rakhra, and M. Bhoyar, "Blockchain-powered solutions for carbon neutral and sustainable economies," in *2025 International Conference on Technology Enabled Economic Changes (InTech)*, IEEE, Feb. 2025, pp. 1510–1515, doi: 10.1109/InTech64186.2025.11198217.

[2] Y. Shang, C. Zhu, Y. Fu, and C. C. Mi, "An integrated heater equalizer for lithium-Ion batteries of electric vehicles," *IEEE Transactions on Industrial Electronics*, vol. 66, no. 6, pp. 4398–4405, 2019, doi: 10.1109/TIE.2018.2863187.

[3] D. Gao, Z. Luo, C. Liu, and S. Fan, "A survey of hybrid energy devices based on supercapacitors," *Green Energy & Environment*, vol. 8, no. 4, pp. 972–988, Aug. 2023, doi: 10.1016/j.gee.2022.02.002.

[4] P. A. N. Denghai, L. V Zejie, and W. U. Yuanzhong, "Sampling circuit, equalization circuit, and system for single cell in series battery pack (U.S," *Patent Application*.

[5] H. Poddar, V. Roy, M. Bhoyar, A. Gangrade, K. N. Venkata Kowshik, and P. Rathod, "Leveraging context-aware fogging for advanced remote patient monitoring and healthcare in modern life," in *2025 4th OPJU International Technology Conference (OTCON) on Smart Computing for Innovation and Advancement in Industry 5.0*, IEEE, Apr. 2025, pp. 1–6, doi: 10.1109/OTCON65728.2025.11070467.

[6] M.-Y. Kim, J.-H. Kim, and G.-W. Moon, "Center-cell concentration structure of a cell-to-cell balancing circuit with a reduced number of switches," *IEEE Transactions on Power Electronics*, vol. 29, no. 10, pp. 5285–5297, Oct. 2014, doi: 10.1109/TPEL.2013.2292078.

[7] C. Lu, L. Kang, S. Wang, Z. Wang, and H. Rao, "A novel inductor-based non-dissipative equalizer," *Energies*, vol. 11, no. 10, Oct. 2018, doi: 10.3390/en11102816.

[8] N. N. Do, H. J. Chiu, and Y. C. Hsieh, "A novel symmetric battery equalizer topology based on bidirectional DC/DC converter for series-connected lithium-ion cells," *2020 3rd International Conference on Power and Energy Applications, ICPEA 2020*, pp. 6–9, 2020, doi: 10.1109/ICPEA49807.2020.9280139.

[9] Y. Li, J. Xu, X. Mei, and J. Wang, "A unitized multiwinding transformer-based equalization method for series-connected battery strings," *IEEE Transactions on Power Electronics*, vol. 34, no. 12, pp. 11981–11989, Dec. 2019, doi: 10.1109/TPEL.2019.2910205.

[10] Z. Huang, S. Yang, S. Wang, W. Yang, and Z. Li, "A novel modularized battery charging and balancing system," *2021 3rd International Conference on Smart Power and Internet Energy Systems, SPIES 2021*, pp. 444–449, 2021, doi: 10.1109/SPIES52282.2021.9633813.

[11] A. F. Moghaddam and A. Van den Bossche, "A single transformer for active cell equalization method of lithium-ion batteries with two times fewer secondaries than cells," *Electronics (Switzerland)*, vol. 8, no. 9, 2019, doi: 10.3390/electronics8090951.

[12] A. F. Moghaddam and A. Van Den Bossche, "A cell equalization method based on resonant switched capacitor balancing for lithium ion batteries," *Proceedings of 2018 9th International Conference on Mechanical and Aerospace Engineering, ICMAE 2018*, pp. 337–341, 2018, doi: 10.1109/ICMAE.2018.8467638.

[13] S. S. Gupta, P. S. Danghi, M. Bhoyar, S. A. A. Ahamed, P. Tanna, and N. Bhaskarani, "Optimizing edge server deployment in 5G networks: a forecasting-based approach with AI-driven strategies," in *2025 4th OPJU International Technology Conference (OTCON) on Smart Computing for Innovation and Advancement in Industry 5.0*, IEEE, Apr. 2025, pp. 1–6, doi: 10.1109/OTCON65728.2025.11070762.

[14] Y. Liu, Y. Huang, H. Zhang, and Q. Huang, "Stability analysis of a phase-shifted full-bridge circuit for electric vehicles based on adaptive neural fuzzy PID control," *Scientific Reports*, vol. 11, no. 1, p. 20040, Oct. 2021, doi: 10.1038/s41598-021-99559-4.

[15] Y. Zhao, Q. Xiao, Z. Zhang, X. Zhao, and D. Lin, "Research on ZVS phase-shifted full-bridge broadband inverter based on auxiliary current source," *Energies*, vol. 15, no. 22, Nov. 2022, doi: 10.3390/en15228661.

[16] J.-M. Kim, J. Lee, K. Ryu, and C.-Y. Won, "Power device temperature-balancing control method for a phase-shift full-bridge converter," *Energies*, vol. 13, no. 7, Apr. 2020, doi: 10.3390/en13071623.
[17] S. L. Mekonnen *et al.*, "Research on phase-shifted full-bridge ZVS DC-DC converter with multi-pulsed load," in *2024 IEEE 10th International Power Electronics and Motion Control Conference (IPEMC2024-ECCE Asia)*, May 2024, pp. 4385–4390, doi: 10.1109/IPEMC-ECCEAsia60879.2024.10567725.
[18] F. E. Gocen, S. B. Ozturk, M. H. Aksit, G. Dugan, B. Cakmak, and C. Demir, "Design and implementation of a full sic-based phase-shifted full-bridge dc-dc converter with nanocrystalline-cored magnetics for railway battery charging applications," *Energies*, vol. 18, no. 15, Jul. 2025, doi: 10.3390/en18153945.
[19] G. Qin, H. Ma, J. Lei, and C. Hao, "Advanced control strategies for enhancing the performance of phase-shifted full-bridge series resonant DC–DC converters in photovoltaic micro-inverters," *Energies*, vol. 18, no. 2, Jan. 2025, doi: 10.3390/en18020387.
[20] B. Gong *et al.*, "Design of a dynamic hybrid compensator for current sharing control of parallel phase-shifted full-bridge converter," *Energies*, vol. 16, no. 5, Feb. 2023, doi: 10.3390/en16052204.
[21] D. Liang, J. Li, and R. Qu, "Sensorless control of permanent magnet synchronous machine based on second-order sliding-mode observer with online resistance estimation," *IEEE Transactions on Industry Applications*, vol. 53, no. 4, pp. 3672–3682, Jul. 2017, doi: 10.1109/TIA.2017.2690218.
[22] G. Ruyuan and D. Fujun, "Design of permanent magnet synchronous motor torque ring controller based on super-twisting sliding mode," *Micromotor*, vol. 51, no. 2, pp. 52–68.
[23] W. Dongling, Z. Chaohui, W. Feiyu, and S. Qiang, "Speed and torque control based on super-twisting sliding mode permanent magnet synchronous motor," *Motor Control and Applications*, vol. 44, no. 10, pp. 42–47.
[24] Z. Zhang *et al.*, "Adaptive fuzzy active-disturbance rejection control-based reconfiguration controller design for aircraft anti-skid braking system," *Actuators*, vol. 10, no. 8, Aug. 2021, doi: 10.3390/act10080201.
[25] X. Yan, J. Sun, Y. Li, J. Qi, and Y. Pan, "Self-adaptive tuning of fuzzy PID control of PV grid-connected inverter," in *2009 Sixth International Conference on Fuzzy Systems and Knowledge Discovery*, Aug. 2009, pp. 160–162, doi: 10.1109/FSKD.2009.647.
[26] S. Mamidala, Y. Venkata Pavan Kumar, and S. Naga Venkata Bramareswara Rao, "Adaptive neuro-fuzzy-inference-system-based energy management in grid-integrated solar PV charging station with improved power quality," *World Electric Vehicle Journal*, vol. 17, no. 3, Mar. 2026, doi: 10.3390/wevj17030138.
[27] M. S. Bahraini, M. J. Mahmoodabadi, and N. Lohse, "Robust adaptive fuzzy fractional control for nonlinear chaotic systems with uncertainties," *Fractal and Fractional*, vol. 7, no. 6, Jun. 2023, doi: 10.3390/fractalfract7060484.
[28] Y. Yang, Y. Wang, W. Zhang, Z. Li, and R. Liang, "Design of adaptive fuzzy sliding-mode control for high-performance islanded inverter in micro-grid," *Energies*, vol. 15, no. 23, Dec. 2022, doi: 10.3390/en15239154.

## BIOGRAPHIES OF AUTHORS



**Pravin Sakharam Wankhade** is currently pursuing a Ph.D. degree at G.H. Raisoni University, Amravati, India, while serving as an assistant professor at Jagadambha College of Engineering and Technology, Yavatmal, India. He holds a master's degree from G.H. Raisoni College of Engineering and Management, Amravati, India. He is a life member of the Indian Society for Technical Education (ISTE). He can be contacted at email: pravinwankhade512@gmail.com.



**Dr. Prema Manoj Daigavane** is a professor and Head of the Department of Electrical Engineering at G.H. Raisoni College of Engineering, Nagpur, India. She received her Ph.D. degree from Nagpur University in 2013. She has published 90 research articles in peer-reviewed journals and conference proceedings. Her research interests include MATLAB applications, fuzzy logic, and image processing. She is a member of the Institution of Engineers (India) and a life member of the Indian Society for Technical Education (ISTE). She can be contacted at email: prema.daigavane@raisoni.net.